Naval Research Laboratory

Washington, DC 20375-5320

NRL/MR/6110--09-9183

EM61-MK2 Response of Three Munitions Surrogates

H.H. NELSON

Chemical Dynamics and Diagnostics Branch
Chemistry Division

T. BELL
J. KINGDON
N. KHADR

SAIC, Inc.
Arlington, Virginia

D.A. STEINHURST

Nova Research, Inc.
Alexandria, Virginia

March 12, 2009

REPORT DOCUMENTATION PAGE

Form Approved
OMB No. 0704-0188

1. REPORT DATE *(DD-MM-YYYY)*	**2. REPORT TYPE**	**3. DATES COVERED** *(From - To)*
12-03-2009	Interim	November 2008 – December 2008

4. TITLE AND SUBTITLE

EM61-MK2 Response of Three Munitions Surrogates

5a. CONTRACT NUMBER
W74RDV73544541

5b. GRANT NUMBER

5c. PROGRAM ELEMENT NUMBER

6. AUTHOR(S)

H.H. Nelson, T. Bell,* J. Kingdon,* N. Khadr,* and D.A. Steinhurst†

5d. PROJECT NUMBER

5e. TASK NUMBER

5f. WORK UNIT NUMBER
61-5802-S-8

7. PERFORMING ORGANIZATION NAME(S) AND ADDRESS(ES)

Naval Research Laboratory, Code 6110
4555 Overlook Avenue, SW
Washington, DC 20375-5320

8. PERFORMING ORGANIZATION REPORT NUMBER

NRL/MR/6110--09-9183

9. SPONSORING / MONITORING AGENCY NAME(S) AND ADDRESS(ES)

Environmental Security Technology
Certification Program
901 North Stuart St., Suite 303
Arlington, VA 22203

10. SPONSOR / MONITOR'S ACRONYM(S)

ESTCP

11. SPONSOR / MONITOR'S REPORT NUMBER(S)

12. DISTRIBUTION / AVAILABILITY STATEMENT

Approved for public release; distribution is unlimited.

13. SUPPLEMENTARY NOTES

*SAIC, Inc., Arlington, VA 22202
†Nova Research Inc., Alexandria, VA 22308

14. ABSTRACT

Target response coefficients for three pipe nipples intended as surrogates for commonly encountered UXO items were calculated from measurements made using the recently developed NRL Time-domain Electromagnetic Induction array. These response coefficients were used to predict the signals expected from an EM61-MK2, the most commonly used geophysical survey instrument for UXO, for each of the three items as a function of orientation and distance of the center of the item below the bottom coil of the sensor. A series of EM61-MK2 survey measurements were made over the surrogates at the NRL Blossom Point Test site to confirm the predictions. The predicted EM61-MK2 signals are presented graphically as plots of the minimum signal expected at the second time gate as a function of distance from the sensor with the confirming survey measurements plotted on the same axes. The minimum signal at each of the four gates available from the EM61-MK2 is tabulated for depths corresponding to 3×, 5×, 7×, and 11× the object's diameter and all the results obtained are attached electronically as a spreadsheet.

15. SUBJECT TERMS
Unexploded Ordnance (UXO)
Electromagnetic Induction (EMI)
Munitions surrogates

16. SECURITY CLASSIFICATION OF:			**17. LIMITATION OF ABSTRACT**	**18. NUMBER OF PAGES**	**19a. NAME OF RESPONSIBLE PERSON**
					Herbert H. Nelson
a. REPORT	**b. ABSTRACT**	**c. THIS PAGE**	UL	19	**19b. TELEPHONE NUMBER** *(include area code)*
Unclassified	Unclassified	Unclassified			(202) 767-3686

CONTENTS

FIGURES

TABLES

EM61-MK2 RESPONSE OF THREE MUNITIONS SURROGATES

INTRODUCTION

The EM61-MK2 Electromagnetic Induction sensor (Geonics Limited, Mississauga, Ontario, Canada) is the most widely used geophysical sensor for unexploded ordnance (UXO) detection surveys. Like all time-domain electromagnetic induction sensors, it produces a pulsed magnetic field (primary field) that induces a secondary field in metallic objects in the vicinity of the sensor. The decay of this induced field is sensed by monitoring the current in a wire-loop receiver coil in four time gates after the turn-off of the primary field. In the EM61-MK2, the main receiver coil is co-located with the transmit coil.

In a typical UXO detection survey, the sensor, with attached wheels or mounted on a cart, is used to survey the field in a raster pattern with a line spacing on the order of the 1-m width of the sensor. Smaller line spacings can be used to increase the data density for more advanced analyses. After data collection, the raw data are typically leveled, background corrected, and mapped. Then, either line-by-line or from a data image, regions of anomalous response are selected and marked as potential metal targets. This initial list of anomalies is used as input to an analysis step that selects anomalies for digging based on features extracted during further analyses such as target size and shape. A target of interest that does not appear on this anomaly list constitutes a detection failure.

One important component of the management of a geophysical investigation is to devise a quality assurance approach that will lead to confidence that the percentage of missed detections is low. Often, this has involved the construction of a geophysical prove-out (GPO) area on the site in which a selection of the targets of interest are buried at a number of different depths and orientations. Each geophysical survey crew is qualified by surveying this area and reporting the number and locations of anomalies detected. Since the identities and locations of the emplaced items in the GPO are blind to the crews, this procedure can serve to validate the survey procedures and data analysis and anomaly detection methods to be used on the site.

This procedure can break down however. The survey crew, who know they are being tested, will always perform with maximum efficiency and care on the GPO but as the production survey proceeds and complacency sets in their performance may slip. If this occurs, the performance measured at the GPO may not be confidently expected in later parts of the survey. This possibility has led a number of site managers and regulators to propose replacing the extensive GPO with a smaller performance confirmation strip, used for a daily confirmation of the survey procedures, coupled with a blind seeding program in the production areas. This approach has the advantage of confirming survey performance as often as a seed is encountered by comparing the measured anomaly location and amplitude to the known values.

Blind seeding, as discussed above, on a large production site will require a large number of items for seeding. One approach is to use inert munitions, matching those expected to be encountered on the site. This is problematic for two reasons. It is often not possible to obtain a sufficient supply of inert munitions at a cost the project can afford. Even if the inert munitions can be found, use of munitions as

Manuscript approved January 29, 2009

seeds requires an extensive inventory and tracking procedure to be implemented; an inert munition left on the site will quite likely trigger a 911 call in the future.

Another, more attractive, approach is to use munitions surrogates (items intended to produce a signature similar to the munitions targets of interest but that do not resemble munitions) as the seed items. If chosen carefully, these surrogates can be widely available and relatively inexpensive. Once the seed items are chosen, the response of the sensor to the items as a function of depth must be determined so that the expected anomaly amplitudes can be predicted.

In an earlier report, we used sensor performance models to predict the response of an EM61-MK2 to a number of common munitions as a function of depth [1]. To validate the results, we collected survey data over those same objects at varying depths and orientations, extracted the maximum signal observed, and compared the measurements to our predictions. In all cases, the model accurately predicts the measured anomaly amplitudes. In this report, we extend this method to three standard steel pipe nipples that we propose for use as surrogates. After a brief description of the model employed and the data collection methodology, we present the predicted and measured anomaly data in graphical and tabular form.

DESCRIPTION OF THE MODEL

The response of a metallic object to an Electromagnetic Induction sensor is most simply modeled as an induced dipole moment represented by a magnetic polarizability matrix $\mathbf{B}$ [2]. As a consequence of electromagnetic reciprocity, the matrix $\mathbf{B}$ is symmetric. By a suitable rotation it can be transformed to diagonal form, so we can write

$$\mathbf{B} = \mathbf{U}\mathbf{B_0}\mathbf{U}^{\mathsf{T}} \tag{1}$$

with

$$\mathbf{B_0} = \begin{bmatrix} \beta_1 & 0 & 0 \\ 0 & \beta_2 & 0 \\ 0 & 0 & \beta_3 \end{bmatrix}. \tag{2}$$

In terms of yaw, pitch and roll Euler angles ϕ, θ and ψ [3], the rotation matrix $\mathbf{U}$ is given by

$$\mathbf{U} = \begin{bmatrix} \cos\theta\cos\phi & \cos\theta\sin\phi & -\sin\theta \\ \sin\psi\sin\theta\cos\phi - \cos\psi\sin\phi & \sin\psi\sin\theta\sin\phi + \cos\psi\cos\phi & \cos\theta\sin\psi \\ \cos\psi\sin\theta\cos\phi + \sin\psi\sin\phi & \cos\psi\sin\theta\sin\phi - \sin\psi\cos\phi & \cos\theta\cos\psi \end{bmatrix}. \tag{3}$$

The eigenvalues β_1, β_2, β_3 correspond to responses induced by the sensor transmit field components aligned with each of the object's principal axes. ϕ, θ and ψ together define the orientations of these principal axes relative to the X, Y and Z coordinate directions. Depending on sensor modality, the βs are functions either of time after the primary field cutoff or of the frequency of the primary field; the Euler angles are not.

In terms of **B** above, the time-domain EMI sensor signal S is modeled as

$$\mathrm{S}(t) = \mu_0 A I_0 \mathbf{C_R} \cdot \mathbf{C_T} \left\{ \frac{d}{dt} \int \hat{I}(t-\tau) \mathbf{B}(\tau) \mathrm{d}\tau \right\} \equiv \mu_0 A I_0 \mathbf{C_R} \cdot \mathbf{C_T} \mathbf{B_E}(t) \qquad (4)$$

In equation (4), μ_0 is the magnetic permeability of free space ($4\pi \mathrm{x} 10^{-7}$ volt-sec/amp-m); A is a scaling factor that depends on the number of turns in the transmit and receive coils, the receiver gain, etc.; I_0 is the peak amplitude of the transmit current pulse; $\mathbf{C}_\mathrm{T}$ and $\mathbf{C}_\mathrm{R}$ are coil sensitivity functions for the transmit and receive coils; and $\mathbf{B_E}$ is the effective polarizability matrix, a quantity which encapsulates the influence of the normalized transmit pulse $\hat{I}(t)$ on **B**. $\mathbf{C}_\mathrm{T}$ and $\mathbf{C}_\mathrm{R}$ depend only on coil geometry and location relative to the object, while **B** depends only on what the object is and how it's oriented, not where it is. The coil sensitivity functions are vectors that specify (a) the strength and direction of the primary field at the object ($\mathbf{C}_\mathrm{T}$) and (b) the sensitivity of the receive coil to the vector components of a magnetic dipole source at the object location ($\mathbf{C}_\mathrm{R}$). The vector $\mathbf{C}_\mathrm{T}\mathbf{B_E}$ describes the strength of the induced object response in the X, Y and Z coordinate directions. Taking the dot product with $\mathbf{C}_\mathrm{R}$ accounts for the relative sensitivity of the receive coil to each of these response components.

The strength and direction of $\mathbf{C}_\mathrm{T}$ and $\mathbf{C}_\mathrm{R}$ are sensitive functions of the location of the EMI sensor relative to the object. $\mathbf{C}_\mathrm{T}$ and $\mathbf{C}_\mathrm{R}$ are defined in terms of integrals around the coil involving the vector from the object to the coil:

$$\mathbf{C}_{\mathbf{T},\mathbf{R}}(\mathbf{r}_0) = \frac{1}{4\pi} \oint_{\mathbf{T},\mathbf{R}} \frac{d\mathbf{l} \times (\mathbf{r}_0 - \mathbf{r})}{|\mathbf{r}_0 - \mathbf{r}|^3} \qquad (5)$$

where $\mathbf{r}_0$ is the location of the object and $\mathbf{r}$ is the location of a point on the coil.

The effective polarizability matrix $\mathbf{B_E}$, as expressed in (4), makes explicit reference to the filtering of **B** via the transmit pulse. However, in general, the situation may further be complicated by the effects of the receiver electronics, which also filter the response. In practice, the latter is accounted for by lumping an object-dependent scale factor into $\mathbf{B_E}$ and using standard test objects to calibrate the sensor by determining A. The eigenvalues (i.e. βs) of the effective polarizability matrix thus become the quantities which we work with.

In general, the aggregate magnitude of the βs determines the size of the object, while differences among the βs relates to the shape of the object. For axially symmetric shapes such as cylinders, prolate or oblate spheroids, and many UXO items, there is a basic longitudinal response along its length and two equal responses transverse to this.

Deriving the βs from EMI data collected over an object is fairly straightforward. As the sensor moves relative to the object, the object is excited from different directions, while the sensitivity of the receiver to the different response components also varies – data from different locations above the object combine the elements of the polarizability matrix $\mathbf{B_E}$ in different ways. As it turns out, if enough data are collected over an area whose dimensions are somewhat larger than the depth of the object, then all of the elements in $\mathbf{B_E}$ contribute enough, and in enough different ways to the overall response that the data can be inverted to determine the βs.

With data collected at N locations ($\mathbf{r}_i$, i=1,2,…,N) over an unknown object, we have an overdetermined set of N simultaneous equations with nine unknown quantities (three βs, three Euler angles that define the object's orientation, and the xyz coordinates of the unknown target location $\mathbf{r}_0$):

$$S_i = \mu_0 A I_0 \mathbf{C_R}(\mathbf{r}_0 - \mathbf{r}_i) \cdot \mathbf{C_T}(\mathbf{r}_0 - \mathbf{r}_i)\mathbf{B_E}, \qquad i=1,2,\ldots,N. \tag{6}$$

The equations are solved in a least-squares sense simultaneously for all values of time. This is accomplished by using a Levenberg-Marquardt gradient search technique to determine the target parameters that minimize the mean squared error between the dipole response model and the measured data.

A key assumption of the dipole response model outlined above is that the behavior with time of the induced currents within an object – from the early surface currents to the later volume currents – is fully embodied in **B** (and hence the βs) defined *at a single point in space*. For the case of a simple compact object sufficiently far from the sensor, this is a very good approximation and can be represented by a unique set of βs. For the case of composite and/or extended objects sufficiently far from the sensor, the model can still give a reasonably good approximation but must now be represented by different sets of βs that depend on the object orientation relative to the sensor.

Note from (4) that for the special case where $\hat{I}(t)$ is an ideal step function, $\mathbf{B_E} \equiv \mathbf{B}$ for all time *t* after the transition from one to zero occurs. For this reason, we refer to the βs from **B** as the *step response* βs and the βs from $\mathbf{B_E}$ as the *effective* βs. Figure 1 below shows plots of the step response and effective βs for a 3" chrome steel and a 4" aluminum sphere. The underlying black curves in each panel represent the step response βs as obtained from theory. Since the sphere is perfectly symmetric, $\beta_1=\beta_2=\beta_3$. Over-plotted in green are the theoretical effective βs for our time-domain electromagnetic sensor (TEM) array (described in the next section) computed solely by convolving the TEM transmit pulse with the step response βs followed by the time derivative, as prescribed by (4). The effective βs derived directly from data taken with the TEM array are shown in red. In this case, the βs (solid, dotted and dashed curves) are essentially identical, as expected. Note that for both the ferrous and nonferrous spheres, the derived effective βs from the TEM array data are an extremely good representation of the step response βs.

For comparison, the magenta curves show the theoretical effective βs for the EM61-MK2. These are computed again as prescribed by (4), but now the pulse being used is that of the EM61-MK2. Note that in this case, the derived effective βs are generally not a good representation of the step response βs. Coincidentally, however, in the regime of the EM61-MK2 time gates (shown as vertical dotted lines), the 3" chrome steel sphere βs are an approximate representation of the step response βs.

Since the EM61-MK2 signal vs depth curves in this report are generated via (4), and step response βs are given as derived from the TEM array data, it will be necessary to accurately convert these to effective βs for the EM61-MK2. A method which appears successful involves fitting each red curve with the sum of a weighted arbitrary number of loops using a procedure developed in SERDP project MM-1313 [4,5]. The cyan curves represent the result of convolving these fitted curves with the EM61-MK2 transmit pulse and taking the time derivative, as prescribed by (4).

Two examples of the predicted EM61-MK2 response in gate 2 are shown in Figure 2. The left panel plots the response expected from a 105mm projectile while the right panel plots the response expected from a 2.75″ rocket warhead. For both cases, the predicted responses are plotted as a function of the distance of the items center below the bottom coil of the sensor. In normal operation, the EM61-MK2 is

deployed on wheels with the bottom coil 42 cm off the ground. For this case, the target depth below the ground will equal the abscissa reading minus 42 cm. Other deployment schemes have the EM61-MK2 sensors mounted on trays that are dragged across the ground. In those cases, a different offset would be applied.

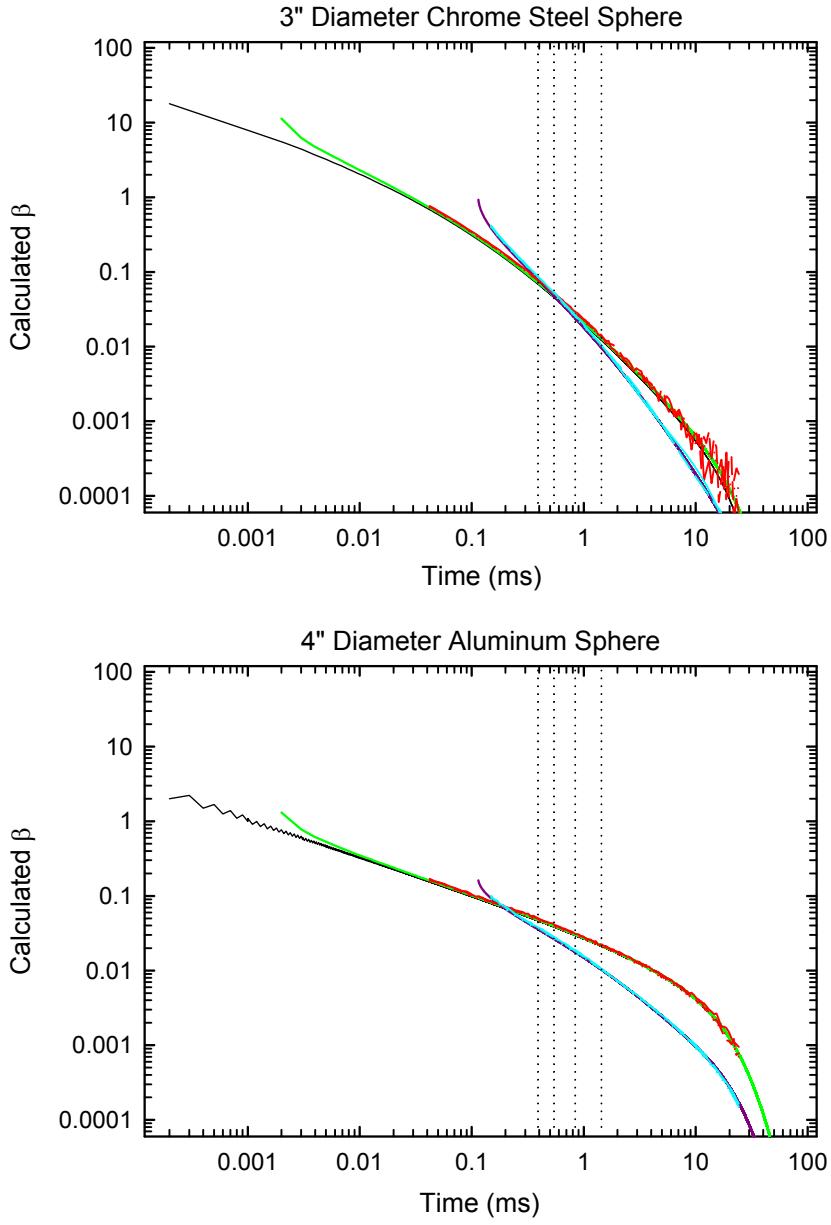

Figure 1 – Step response and effective βs for a 3" chrome steel and a 4" aluminum sphere. The underlying black curves represent the step response βs based on theory; the red curves represent the effective TEM array βs inverted from data; and the cyan curves represent the effective EM61-MK2 βs computed using the effective TEM array βs. Please refer to the text for a full description of the method used. The vertical dotted lines represent the EM61-MK2 *4-channel mode* time gates.

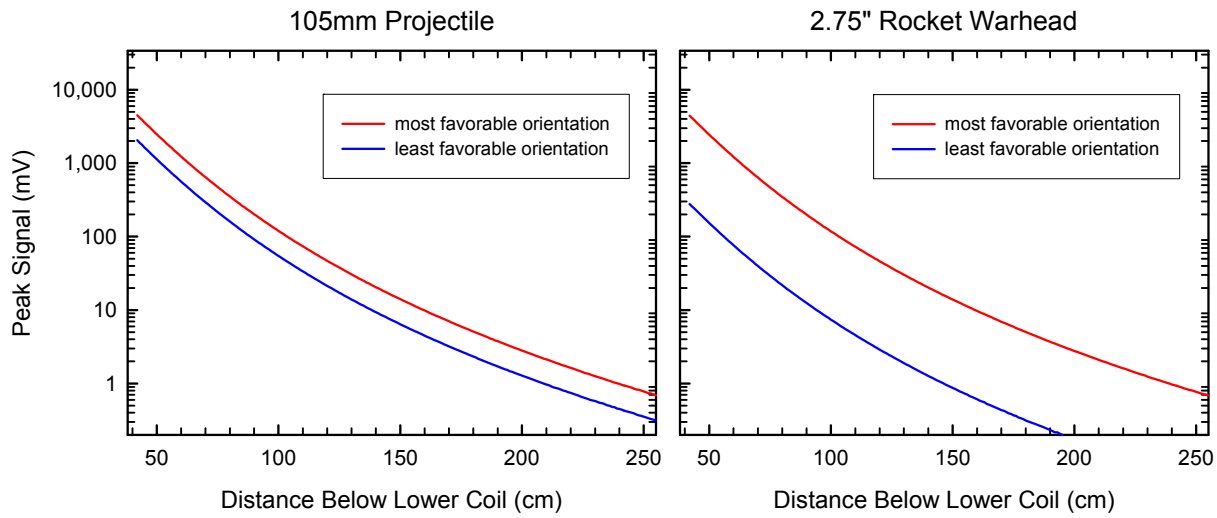

Figure 2 – Predicted EM61-MK2 signal at the second time gate as a function of depth for a 105-mm projectile (left) and a 2.75" rocket warhead (right). In both cases, the response to the object in its most favorable orientation is plotted as a red line and the least favorable orientation as a blue line.

For both items, the predicted response when the item is in its most favorable orientation (oriented vertically under the sensor) is plotted as a red line and that when the item is in its least favorable orientation (oriented horizontally under the sensor perpendicular to the sensor track) as a blue line. The length to diameter aspect ratio of the rocket warhead is substantially larger than that of the projectile accounting for the greater spread between the two responses in the right panel. The long axis of both targets is of similar size yielding similar responses in the most favorable orientation. Except in the most unfavorable conditions, site noise is typically 1 mV or below allowing both of these items to be detected at depths approaching 1 m under standard deployment conditions.

MUNITIONS SURROGATES

In keeping with our goal of widely available and inexpensive surrogates, we have chosen to use pipe nipples. Each of the three surrogates employed is a black, welded steel, Schedule 40 straight pipe nipple, threaded on both ends. We obtained the samples for this study on-line from McMaster-Carr (http://www.mcmaster.com/) but they are widely available from a variety of sources. The details of the three surrogates are given in Table 1.

Table 1. Munitions Surrogates Used in this Work.

Item	Nominal Pipe Size	Outside Diameter	Length	Part Number
Small Surrogate	1"	1.315" (33.4 mm)	4"	44615K466
Medium Surrogate	2"	2.375" (60.3 mm)	8"	44615K529
Large Surrogate	4"	4.500" (114.3 mm)	12"	44615K137

DATA COLLECTION PROCEDURES

Two data collections were carried out for each of the munitions items studied. Although the target response coefficients needed to predict the sensor signal as a function of depth can be determined from a series of EM61-MK2 measurements, it proved to be more efficient to determine the βs using our TEM array using the procedures outlined above. This instrument, developed with ESTCP support, comprises a five-by-five array of time-domain EM sensors each consisting of a 35-cm transmit coil and an inner 25-cm receive coil, Figure 3. With the munitions item to be investigated placed under the center sensor in the array, the transmit coils are energized sequentially and decay data are collected from all 25 receive coils; 625 individual decays in total, from 40 μs to 25 ms after the primary is turned off.

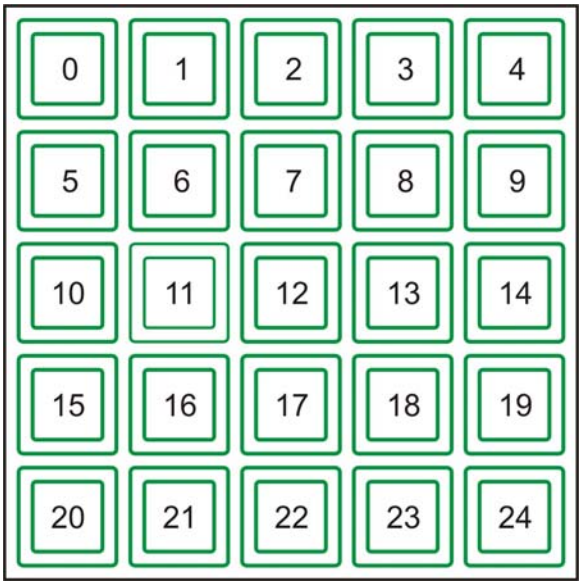

Figure 3 – Schematic of the 25-element TEM array used to determine the response coefficients of the test objects

A small subset of the data collected from a 2.75-in warhead oriented horizontally along track 35cm below the sensor array is shown in Figure 4. The nine decay curves shown are the response measured at the nine central receivers when the corresponding transmit coil is energized (monostatic response). Some of the shape information available from these sensors is evident in the plot. The decays measured using sensors 7 and 17, which primarily excite longitudinal modes of a prolate spheroidal target oriented along track, have distinct decay behavior from sensors 11 and 13, which primarily excite transverse modes.

TEM array data were collected from each of the three surrogates at different target orientations. These data were inverted for target response coefficients, β, as described above. Combined with the known transmit and receive properties of the EM61-MK2, these βs were used to predict the sensor response to the three items as a function of depth.

In order to validate these predictions, EM61-MK2 surveys were conducted over each of the surrogates positioned at a variety of depths and orientations in our test pit at Blossom Point. These surveys consisted of a single pass of the sensor at normal survey speed over the object starting ten meters in front of the pit and continuing ten meters past the pit. Before and after each series of measurements, data were collected over the empty pit to ensure that the sensor background was at reasonable levels. The

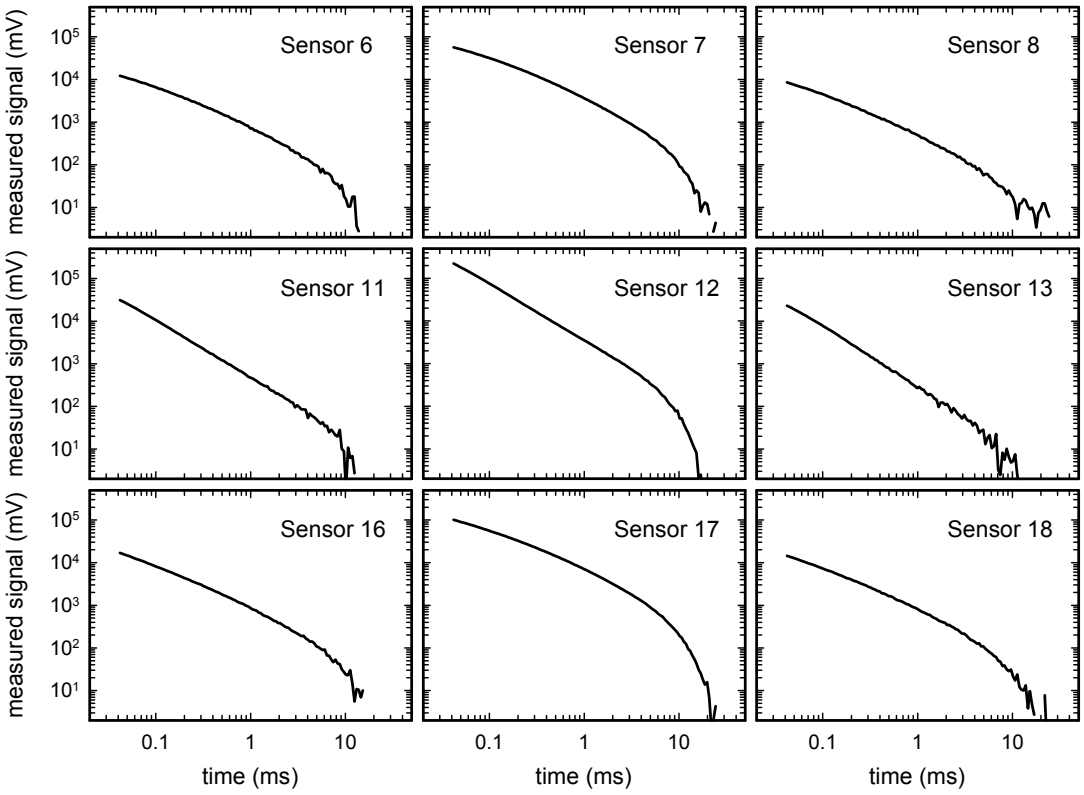

Figure 4 – Measured response of a 2.75-in warhead oriented horizontally along track 35 cm below the TEM array. The nine decays shown represent the response of the nine central receivers (see Figure 1) when the corresponding transmitter is energized.

survey data were background corrected using data collected before and after the test pit and the largest amplitude signal for each of the four time gates selected. In many cases this is not the measurement directly above the object; for a cylinder placed flat and oriented along the survey track, the peak signals are observed before and after the object. Each object was measured at nine to twelve unique position/orientation combinations.

For all EM61-MK2 data reported in this report, the sensor was operated in 4-channel or "4" mode with four sampling gates devoted to the lower, primary receive coil. The nominal delay time from the initial turn-off of current to the coil for each of the four gates is listed in Table 2. A standard EM61-MK2 was used for this work; the instrument manual lists delays from complete turn-off of current.

Table 2. Nominal delay time and receive coil used for each of the EM61-MK2 gates in "4 channel" mode

Gate	Receive Coil	Nominal Delay
1	Lower	216 μs
2	Lower	366 μs
3	Lower	660 μs
4	Lower	1266 μs

RESULTS

The results of this investigation are shown in Figures 5 through 7. For each of the figures, the top panel is a photograph of the actual item measured and the bottom panel shows the predicted and measured EM61-MK2 response at the second time gate. The predicted response when the item is in its least favorable orientation is plotted as a solid blue line. Measured responses are plotted as crosses. In all cases, the measured responses are described well by the calculated curve. The system noise, which limits the ultimate depth of detection of the item under investigation, determined at the site is plotted as a dash-dot line. The RMS noise at this site was 0.5 mV for gate 2 but this is a strong function of the roughness of the terrain and may be higher at other sites. The observed static and moving RMS noise amplitudes for all gates are given in Table 3.

Table 3. Measured RMS noise for each of the four gates in static and survey mode.

Gate	Static (mV)	Survey (mV)
1	0.5	0.8
2	0.1	0.5
3	0.2	0.4
4	0.3	0.3

The minimum signals predicted for all three surrogates investigated for all four gates for depths corresponding to 3x, 5x, 7x, and 11x the items diameter are tabulated in Table 4. All predicted sensor responses are tabulated in a spreadsheet which is attached electronically as Appendix A.

The results presented here are for data collected when the test object passes directly under the middle of the sensor. Depending on the objectives of a particular survey (detection vs. classification, large deep items vs. small shallow items) the survey lane spacing chosen may result in some potential targets passing off-center under the sensor. Figure 8 plots the measured signals from a test sphere and the small surrogate as a function of distance from the center of the sensor. In each case, the items were positioned with their center 50 cm below the lower coil of the EM61-MK2.

The upper panel of Figure 8 shows the response from a standard 4-in aluminum sphere. As expected, the response is relatively constant near the center of the coil and then begins to fall off as the sphere approaches and then passes outside the edge of the coil which is indicated with a dotted line. The lower panel plots the response of the small surrogate oriented along- and across-track with the scaled response of the sphere for reference. The surrogate oriented along track results in fall-off behavior that matches the sphere data. As the across-track surrogate is moved toward the edge of the transmit coil, more of the long-axis response of the pipe is excited and the signal rises dramatically before beginning to fall as the surrogate moves outside the sensor coil.

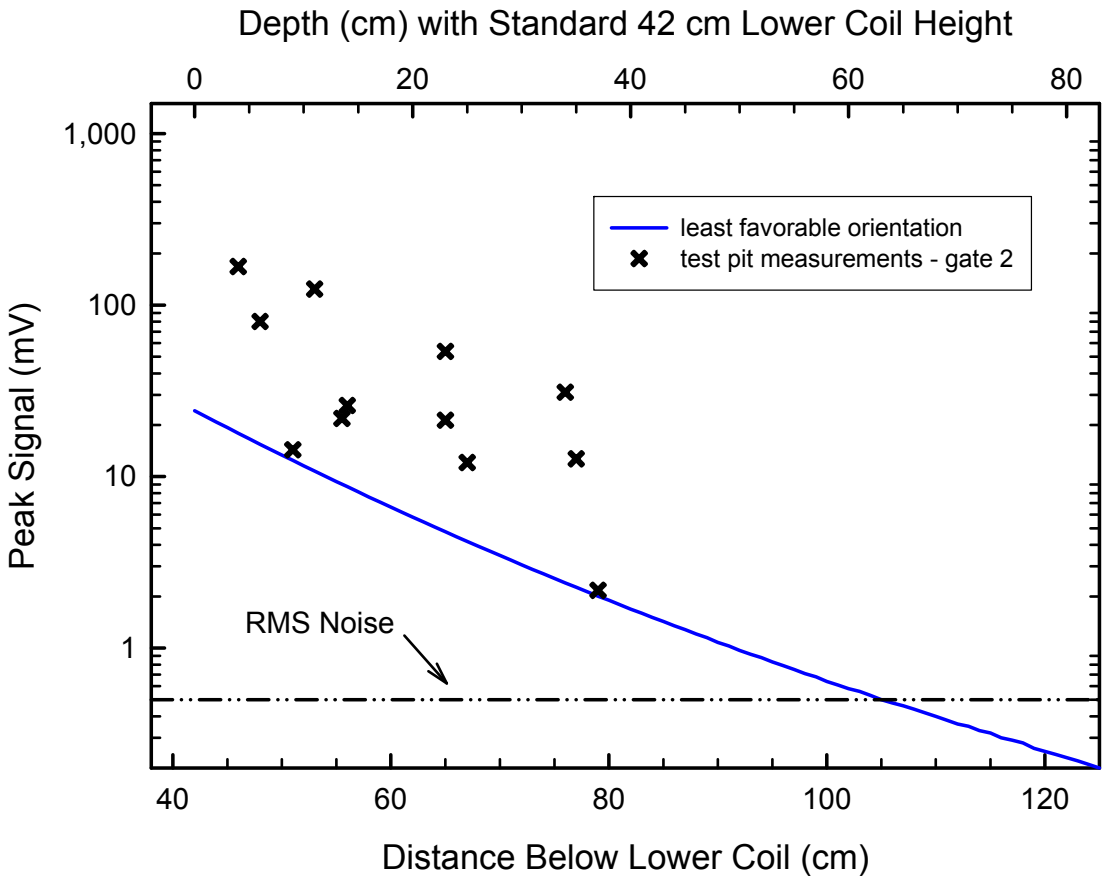

Figure 5 – EM61-MK2 signal at the second time gate as a function of the distance of the center of a small munitions surrogate below the sensor's bottom coil. The predicted response to the object in its least favorable orientation is shown as a solid line, test pit measurements are plotted as crosses, and the site noise is shown as a dot-dash line.

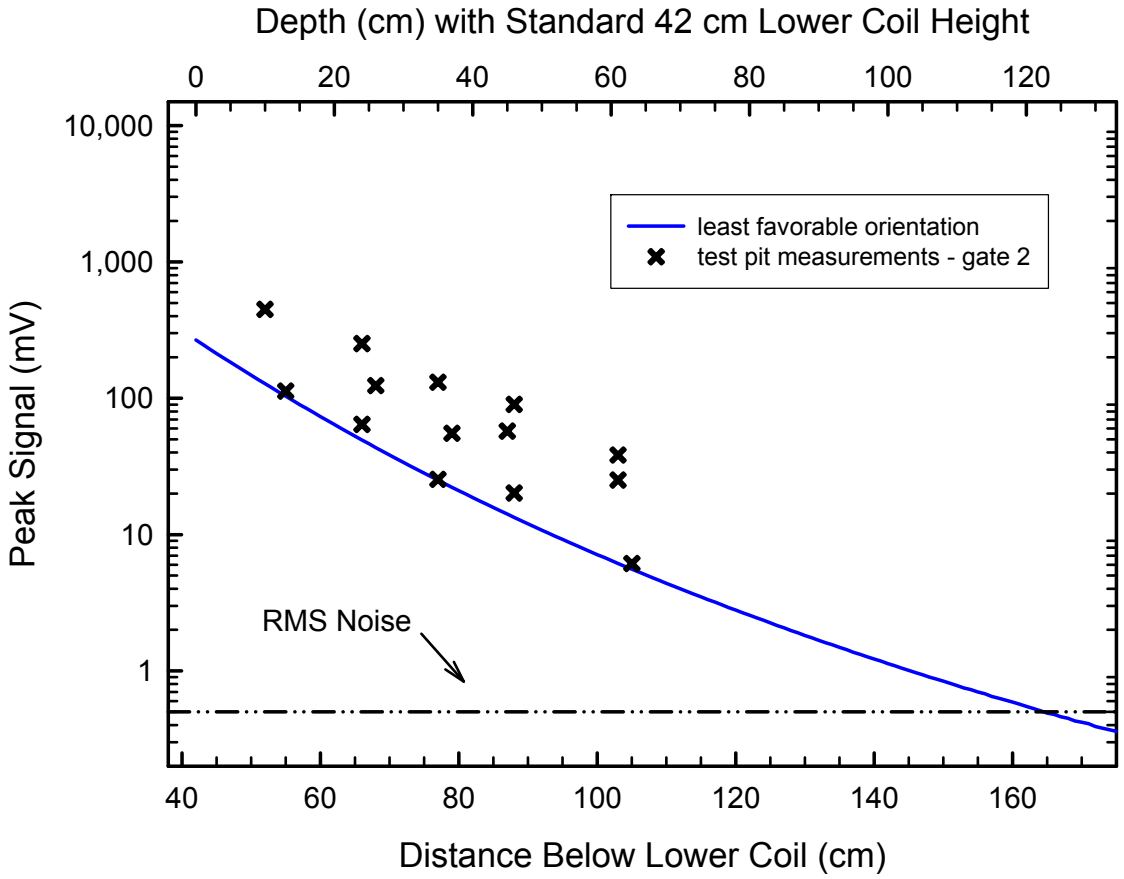

Figure 6 – EM61-MK2 signal at the second time gate as a function of the distance of the center of a medium-sized munitions surrogate below the sensor's bottom coil. The predicted response to the object in its least favorable orientation is shown as a solid line, test pit measurements are plotted as crosses, and the site noise is shown as a dot-dash line.

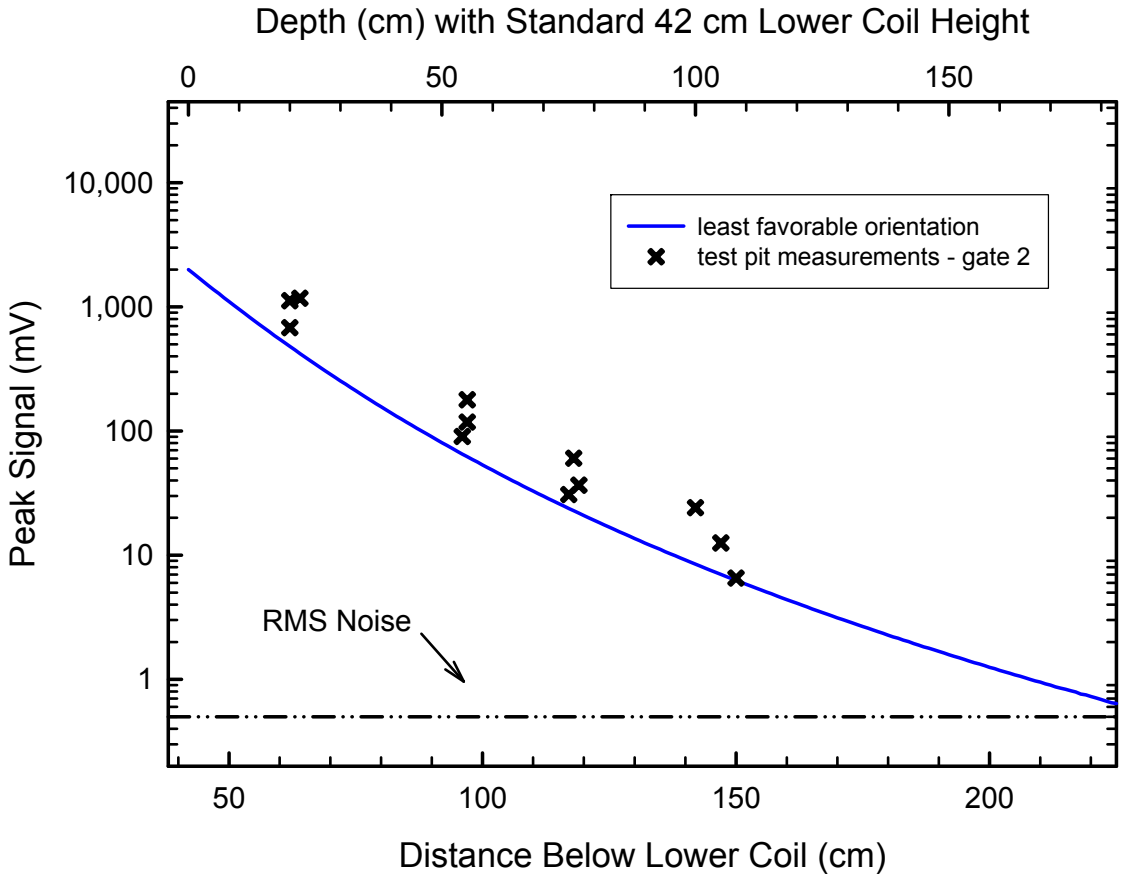

Figure 7 – EM61-MK2 signal at the second time gate as a function of the distance of the center of a large munition surrogate below the sensor's bottom coil. The predicted response to the object in its least favorable orientation is shown as a solid line, test pit measurements are plotted as crosses, and the site noise is shown as a dot-dash line.

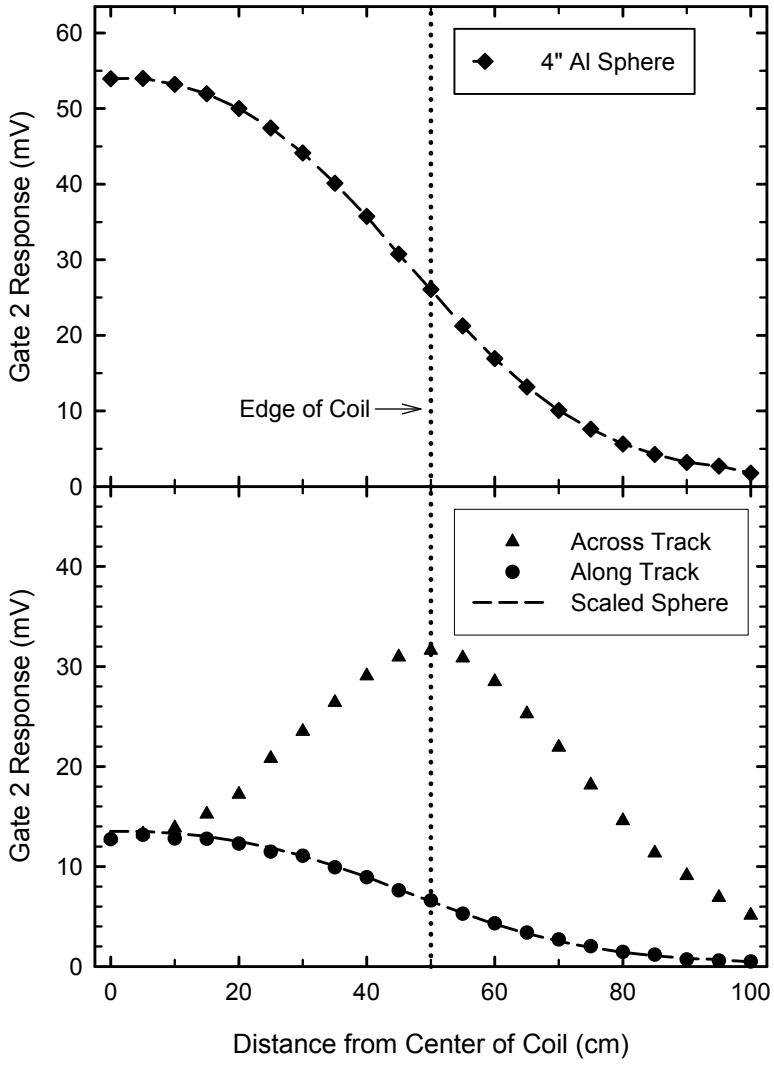

Figure 8 – Test item response as a function of cross-track distance from the center of an EM61-MK2 oriented with the 1-m axis perpendicular to the survey direction. The top panel shows the response of a 4-in aluminum sphere located 50 cm below the lower coil. The bottom panel shows the response of the small surrogate oriented both along the direction of survey and across the direction of survey. The scaled response of the sphere is shown for reference. In both panels, the edge of the sensor coil is indicated by a dotted line.

Table 4. Predicted minimum EM61-MK2 signal for the three munitions surrogates at a depth corresponding to 3x, 5x, 7x, and 11x their respective diameter. The sensor is assumed to be deployed on its standard wheels which correspond to the bottom coil 42 cm above the ground.

Item	Depth (cm)	Gate 1 (mV)	Gate 2 (mV)	Gate 3 (mV)	Gate 4 (mV)
3x Depth					
Small Surrogate	10	20.9	11.6	5.2	1.8
Medium Surrogate	18	131	73.4	33.2	12.7
Large Surrogate	34	324	199	98.8	40.2
5x Depth					
Small Surrogate	17	12.8	7.1	3.2	1.1
Medium Surrogate	30	60.4	33.9	15.3	5.8
Large Surrogate	57	91.6	56.1	27.9	11.3
7x Depth					
Small Surrogate	23	8.6	4.8	2.1	0.8
Medium Surrogate	42	29.8	16.7	7.6	2.9
Large Surrogate	80	31.2	19.1	9.5	3.9
11x Depth					
Small Surrogate	37	3.6	2.0	0.9	0.3
Medium Surrogate	66	8.6	4.8	2.2	0.8
Large Surrogate	128	5.1	3.1	1.6	0.6

SUMMARY

We have used the NRL TEM Array to characterize three standard pipe nipples intended to serve as surrogates for munitions items commonly found on Military Munitions Response Sites. Using these data we have determined EM response coefficients for each object. These response coefficients have been used to calculate the expected signal from an EM61-MK2 over each surrogate as a function of depth and orientation. These results have been presented graphically and the minimum signal expected at a depth corresponding to 3x, 5x, 7x, and 11x the objects diameter has been tabulated.

REFERENCES

1. Nelson, H. H., Bell, T., Kingdon, J., Khadr, N., and Steinhurst, D.A., "EM61-MK2 Response of Standard Munitions Items," NRL/MR/6110--08-9155, October 6, 2008.

2. Baum, C. (ed.), Detection and Identification of Visually Obscured Targets, Taylor and Francis, 1999.

3. Goldstein, H., Classical Mechanics, 2nd ed., Addison-Wesley, 1980.

4. Miller, J., and Furuya, T., "Variability of Real UXO," Symposium on the Application of Geophysics to Engineering and Environmental Problems 2007, Denver CO.

5. Miller, J., and Kingdon, J., "Quantification of UXO Variability for Target Discrimination," UXO Forum 2006, Las Vegas, NV.